Inorg. Chem. **2008**, *47*, 6763−6770

Ternary Rare-Earth Titanium Antimonides $RE_2Ti_{11-x}Sb_{14+x}$ (*RE* = Sm, Gd, Tb, Yb)

Haiying Bie and Arthur Mar*

Department of Chemistry, University of Alberta, Edmonton, Alberta, Canada T6G 2G2

Received February 20, 2008

The isostructural rare-earth titanium antimonides $RE_2Ti_{11-x}Sb_{14+x}$ (*RE* = Sm, Gd, Tb, Yb) have been synthesized by arc-melting reactions of the elements. Single-crystal X-ray diffraction revealed that they adopt a new structure type (Pearson symbol *oP*54, space group *Pnma*, $Z = 2$; $a = 15.8865(6)-15.9529(9)$ Å, $b = 5.7164(2)-5.7135(3)$ Å, $c = 12.9244(5)-12.9442(7)$ Å for *RE* = Sm−Yb). The structure consists of titanium-centered octahedra (CN6) and pentagonal bipyramids (CN7) connected to form a 3D framework whose cavities are filled with *RE* atoms. 1D linear skewers of titanium atoms, within face-sharing octahedral chains, and similar skewers of antimony atoms, associated with the titanium-centered pentagonal bipyramids, extend along the *b* direction. On proceeding from $Sm_2Ti_{11}Sb_{14}$ to $Tb_2Ti_{10.41(1)}Sb_{14.59(1)}$ and $Yb_2Ti_{10.58(1)}Sb_{14.42(1)}$, antimony atoms are disordered within some of the titanium sites. Resistivity measurements on the samarium and ytterbium members indicated metallic behavior.

Introduction

Ternary rare-earth transition-metal antimonides *RE*−M−Sb form an attractive class of materials for discovering new structure types and unusual physical properties.[1] In contrast to compounds of the lighter pnicogens, these antimonides tend to adopt structures containing polyhedra with higher CN (because of the large size of antimony) and with greater likelihood of disorder. Much of the current interest in ternary rare-earth antimonides relates to the search for new thermoelectric materials,[2] but they also display diverse electrical and magnetic properties.[3] Although systems containing a late transition metal are now relatively well-known, those containing an early transition metal remain sparsely investigated.

In the *RE*−Ti−Sb systems, the existence of two phases has now been established for the earlier *RE* metals: RE_3TiSb_5 (*RE* = La−Nd, Sm)[4,5] and $RE_2Ti_7Sb_{12}$ (*RE* = La−Nd).[6] A tin-stabilized phase, $RETi_3(Sn_xSb_{1-x})_4$ ($x = 0.1$), also forms for *RE* = Nd and Sm.[6] No other ternary phases were revealed in the La−Ti−Sb phase diagram at 800 °C besides the two indicated above.[6] Although no ternary phases were found in the Er−Ti−Sb phase diagram,[6] it is not clear if this also holds true for other systems containing a later *RE* metal. Here, we describe the synthesis of a new phase, $RE_2Ti_{11-x}Sb_{14+x}$, which forms for *RE* = Sm, Gd, Tb, and Yb. The structure type is new, featuring a complex framework built up from six- and seven-coordinate titanium-centered polyhedra.

Experimental Section

Synthesis. In attempts to extend the $RE_2Ti_7Sb_{12}$ (*RE* = La−Nd) series to later *RE* members, a new phase was identified in a reaction intended to prepare "$Sm_2Ti_7Sb_{12}$", as determined by powder X-ray diffraction and energy-dispersive X-ray (EDX) analysis. Similar reactions were carried out for *RE* = Gd−Er and Yb but were successful for only *RE* = Gd, Tb, and Yb. Reactions were conducted by arc-melting mixtures of the elements with overall stoichiometry "$RE_2Ti_7Sb_{12}$" (or 9% *RE*, 34% Ti, 57% Sb) in an Edmund Bühler MAM-1 compact arc melter on a water-cooled copper block under an argon atmosphere gettered with titanium. Starting materials were pieces of the rare-earth elements (99.9%, Hefa), titanium sponge (99.9%, Fisher), and antimony pieces (99.999%, Alfa-Aesar). A 5 wt % excess of antimony was added to compensate for its

* To whom correspondence should be addressed. E-mail: arthur.mar@ualberta.ca.

(1) Sologub, O. L.; Salamakha, P. S. In *Handbook on the Physics and Chemistry of Rare Earths*; Gschneidner, K. A., Jr., Bünzli J.-C. G., Pecharsky, V. K., Eds.; Elsevier: Amsterdam, 2003; Vol. 33, pp 35−146.
(2) Brown, S. R.; Kauzlarich, S. M.; Gascoin, F.; Snyder, G. J. *Chem. Mater.* **2006**, *18*, 1873–1877.
(3) Wakeshima, M.; Sakai, C.; Hinatsu, Y. *J. Phys.: Condens. Matter* **2007**, *19*, 016218-1–016218-10.
(4) Bolloré, G.; Ferguson, M. J.; Hushagen, R. W.; Mar, A. *Chem. Mater.* **1995**, *7*, 2229–2231.
(5) Moore, S. H. D.; Deakin, L.; Ferguson, M. J.; Mar, A. *Chem. Mater.* **2002**, *14*, 4867–4873.
(6) Bie, H.; Moore, S. H. D.; Piercey, D. G.; Tkachuk, A. V.; Zelinska, O. Ya.; Mar, A. *J. Solid State Chem.* **2007**, *180*, 2216–2224.

10.1021/ic800317c CCC: $40.75
Published on Web 07/11/2008

Table 1. Crystallographic Data for $RE_2Ti_{11-x}Sb_{14+x}$ (RE = Sm, Tb, Yb)

formula	$Sm_2Ti_{11}Sb_{14}$	$Tb_2Ti_{10.41(1)}Sb_{14.59(1)}$	$Yb_2Ti_{10.58(1)}Sb_{14.42(1)}$
fw (amu)	2532.10	2593.55	2608.87
space group	*Pnma* (No. 62)	*Pnma* (No. 62)	*Pnma* (No. 62)
a (Å)	15.8865(6)	15.8693(18)	15.9529(9)
b (Å)	5.7164(2)	5.7036(6)	5.7135(3)
c (Å)	12.9244(5)	12.9309(15)	12.9442(7)
V (Å^3)	1173.71(8)	1170.4(2)	1179.82(11)
Z	2	2	2
ρ_{calcd} (g cm^{-3})	7.165	7.359	7.344
cryst dimensions (mm^3)	0.23 × 0.07 × 0.06	0.11 × 0.08 × 0.05	0.19 × 0.12 × 0.06
radiation	graphite monochromated Mo $K\alpha$, λ = 0.71073 Å		
μ(Mo $K\alpha$) (mm^{-1})	24.19	25.77	27.35
transmission factors	0.056−0.282	0.076−0.292	0.043−0.248
2θ limits	4.06° ≤ 2θ(Mo $K\alpha$) ≤ 66.28°	4.06° ≤ 2θ(Mo $K\alpha$) ≤ 66.26°	4.06° ≤ 2θ(Mo $K\alpha$) ≤ 66.24°
data collected	$-23 \le h \le 23$, $-8 \le k \le 8$, $-19 \le l \le 19$	$-24 \le h \le 24$, $-8 \le k \le 8$, $-19 \le l \le 19$	$-23 \le h \le 24$, $-8 \le k \le 8$, $-19 \le l \le 19$
no. of data collected	15 628	15 600	15 686
no. of unique data, including $F_o^2 < 0$	2403 (R_{int} = 0.038)	2396 (R_{int} = 0.082)	2410 (R_{int} = 0.036)
no. of unique data, with $F_o^2 > 2\sigma(F_o^2)$	2194	1866	2179
no. of variables	92	92	93
$R(F)$ for $F_o^2 > 2\sigma(F_o^2)$ [a]	0.019	0.033	0.024
$R_w(F_o^2)$ [b]	0.042	0.061	0.050
GOF	1.101	1.052	1.151
$(\Delta\rho)_{max}$, $(\Delta\rho)_{min}$ (e Å^{-3})	1.06, −1.64	2.19, −2.12	1.50, −2.02

[a] $R(F) = \sum||F_o| - |F_c||/\sum|F_o|$. [b] $R_w(F_o^2) = [\sum[w(F_o^2 - F_c^2)^2]/\sum w F_o^4]^{1/2}$; $w^{-1} = [\sigma^2(F_o^2) + (Ap)^2 + Bp]$ where $p = [\max(F_o^2,0)+2F_c^2]/3$.

volatilization during arc-melting, and the alloys were melted twice to ensure homogeneity. The powder X-ray diffraction patterns of the as-melted ingots, obtained on an Inel powder diffractometer equipped with a CPS 120 detector, were in good agreement with those calculated from the single-crystal data (described below).

Single crystals of the title compounds were obtained after annealing the arc-melted samples, which were placed within alumina crucibles and then sealed within fused-silica tubes under vacuum. The tubes were heated to 650 °C over 1 day, heated to 1050 °C over 1 day, kept at that temperature for 2 days, slowly cooled to 800 °C over 4 days, kept at that temperature for 12 days, and then slowly cooled to 20 °C over 4 days. EDX analyses on these crystals with a Hitachi S-2700 scanning electron microscope gave approximate chemical compositions (8−13% *RE*, 38−43% Ti, 46−52% Sb) that were consistent with the formulas ultimately refined from the structure determinations. The ideal elemental composition for $RE_2Ti_{11}Sb_{14}$ (7% *RE*, 41% Ti, 52% Sb) is not readily distinguishable from that for $RE_2Ti_7Sb_{12}$ (9% *RE*, 34% Ti, 57% Sb), given that the uncertainties in semiquantitative EDX analyses can be as high as ∼5%. For $Gd_2Ti_{11-x}Sb_{14+x}$, suitable samples for single-crystal X-ray diffraction were unavailable, but its unit cell parameters refined from the powder X-ray diffraction pattern were found to be a = 15.899(1) Å, b = 5.7198(5) Å, and c = 12.938(1) Å.

In lieu of arc-melting, direct reactions of the elements close to the loading composition $RE_2Ti_{11}Sb_{14}$ (RE = Sm, Gd−Er, Yb) with a similar heating profile as above have also been attempted. These reactions generally resulted in the formation of binary phases, except for the occasional observation of small crystals of the ternary phase in the case of RE = Yb. Given that ytterbium has the lowest melting point of the late *RE* metals, we cannot rule out the possibility that the other ternary phases, including those of the missing *RE* members, may be accessible through a different heating treatment. Further experiments are in progress to test this hypothesis.

Structure Determination. Single-crystal X-ray diffraction data were collected on a Bruker Platform/SMART 1000 CCD diffractometer at 22 °C using ω scans. Structure solution and refinement were carried out with use of the *SHELXTL* (version 6.12) program package.[7] Face-indexed numerical absorption corrections were applied. Crystal data and further details of the data collection are given in Table 1.

For $Sm_2Ti_{11}Sb_{14}$, the intensity pattern and statistics favored the centrosymmetric orthorhombic space group *Pnma*. Initial atomic positions for the samarium, titanium, and most of the antimony atoms were found by direct methods. The difference electron density map revealed additional peaks, which were assigned as two sets of split antimony sites: Sb5/Sb6 and Sb7/Sb8. When allowed to refine freely and no restrictions are placed on the total occupancy within a set of split antimony sites, the occupancies converged to 0.52(2) for Sb5, 0.48(2) for Sb6, 0.53(2) for Sb7, and 0.47(2) for Sb8. In subsequent refinements, these occupancies were fixed at exactly 0.50. All other sites were found to be fully occupied except for Ti5, which exhibited an anomalously large displacement parameter and which is located too close to Sb6 (2.36 Å) and Sb7 (2.30 Å). The occupancy of Ti5 converged to 0.44(1) when refined but was fixed at exactly 0.50 to simplify interpretation of the disorder inherent in the crystal structure, as described later. Intensity data on the same crystal were recollected to determine if site ordering sets in at low temperature (−80 °C). However, these data led to essentially the same disordered structure solution as at room temperature.

Other subgroups of *Pnma* were considered ($P2_12_12_1$, $P2_1/c$, $P2_1/m$, $Pmn2_1$, $Pna2_1$, and $Pmc2_1$) to ascertain if the disorder problems result from an incorrect choice of space group with too high symmetry. In all cases, the same features of split antimony sites and partial Ti5 occupancy persist. Careful re-examination of the CCD frames of intensity data for the original crystal as well as other separately mounted crystals also provided no evidence for superstructure reflections.

Similar procedures applied to the data sets for the terbium and ytterbium compounds revealed that some of the other titanium sites had unusually small displacement parameters, suggesting that they are disordered with antimony atoms. In the terbium compound, the *M*3 site contains 0.85 Ti and 0.15 Sb, corresponding to an overall

(7) Sheldrick, G. M. *SHELXTL, Version 6.12*; Bruker AXS Inc.: Madison, WI, 2001.

Table 2. Atomic Coordinates and Equivalent Isotropic Displacement Parameters for $RE_2Ti_{11-x}Sb_{14+x}$ (RE = Sm, Tb, Yb)

atom	Wyckoff position	occupancy	x	y	z	U_{eq} (Å^2)[a]
$Sm_2Ti_{11}Sb_{14}$						
Sm	4*c*	1	0.3619(1)	1/4	0.0530(1)	0.0110(1)
Ti1	4*c*	1	0.3745(1)	1/4	0.7064(1)	0.0122(2)
Ti2	4*c*	1	0.0870(1)	1/4	0.7532(1)	0.0115(1)
Ti3	8*d*	1	0.3520(1)	0.0073(1)	0.4860(1)	0.0096(1)
Ti4	4*c*	1	0.1881(1)	1/4	0.3718(1)	0.0108(1)
Ti5	4*c*	0.50	0.0156(1)	1/4	0.1525(2)	0.0222(4)
Sb1	4*c*	1	0.2494(1)	1/4	0.8516(1)	0.0095(1)
Sb2	4*c*	1	0.4980(1)	1/4	0.5622(1)	0.0114(1)
Sb3	4*c*	1	0.2127(1)	1/4	0.5858(1)	0.0104(1)
Sb4	8*d*	1	0.0322(1)	0.5001(1)	0.3688(1)	0.0116(1)
Sb5	4*c*	0.50	0.3511(1)	1/4	0.2906(2)	0.0103(3)
Sb6	4*c*	0.50	0.3720(1)	1/4	0.3012(2)	0.0100(2)
Sb7	4*c*	0.50	0.1601(1)	1/4	0.1637(1)	0.0104(2)
Sb8	4*c*	0.50	0.1867(1)	1/4	0.1623(1)	0.0113(2)
$Tb_2Ti_{10.41(1)}Sb_{14.59(1)}$						
Tb	4*c*	1	0.3618(1)	1/4	0.0531(1)	0.0096(1)
Ti1	4*c*	1	0.3743(1)	1/4	0.7053(1)	0.0082(3)
Ti2	4*c*	1	0.0878(1)	1/4	0.7525(1)	0.0053(3)
*M*3	8*d*	0.853(3) Ti, 0.147(3) Sb	0.3511(1)	0.0080(1)	0.4860(1)	0.0063(3)
Ti4	4*c*	1	0.1880(1)	1/4	0.3728(1)	0.0081(3)
Ti5	4*c*	0.50	0.0161(2)	1/4	0.1532(2)	0.0118(6)
Sb1	4*c*	1	0.2505(1)	1/4	0.8520(1)	0.0082(1)
Sb2	4*c*	1	0.4980(1)	1/4	0.5621(1)	0.0086(1)
Sb3	4*c*	1	0.2114(1)	1/4	0.5859(1)	0.0088(1)
Sb4	8*d*	1	0.0320(1)	0.5002(1)	0.3703(1)	0.0104(1)
Sb5	4*c*	0.50	0.3502(2)	1/4	0.2889(4)	0.0087(5)
Sb6	4*c*	0.50	0.3718(2)	1/4	0.2999(4)	0.0096(5)
Sb7	4*c*	0.50	0.1609(1)	1/4	0.1639(2)	0.0099(4)
Sb8	4*c*	0.50	0.1887(1)	1/4	0.1625(2)	0.0087(4)
$Yb_2Ti_{10.58(1)}Sb_{14.42(1)}$						
Yb	4*c*	1	0.3634(1)	1/4	0.0518(1)	0.0139(1)
Ti1	4*c*	1	0.3723(1)	1/4	0.7058(1)	0.0132(2)
*M*2	4*c*	0.789(3) Ti, 0.211(3) Sb	0.0897(1)	1/4	0.7498(1)	0.0134(2)
Ti3	8*d*	1	0.3517(1)	0.0062(1)	0.4855(1)	0.0108(1)
Ti4	4*c*	1	0.1880(1)	1/4	0.3709(1)	0.0121(2)
Ti5	4*c*	0.50	0.0162(1)	1/4	0.1546(2)	0.0120(3)
Sb1	4*c*	1	0.2499(1)	1/4	0.8524(1)	0.0118(1)
Sb2	4*c*	1	0.4975(1)	1/4	0.5630(1)	0.0116(1)
Sb3	4*c*	1	0.2133(1)	1/4	0.5838(1)	0.0134(1)
Sb4	8*d*	1	0.0328(1)	0.0006(1)	0.3672(1)	0.0138(1)
Sb5	4*c*	0.50	0.3497(1)	1/4	0.2898(2)	0.0117(3)
Sb6	4*c*	0.50	0.3709(1)	1/4	0.3003(2)	0.0133(2)
Sb7	4*c*	0.50	0.1600(1)	1/4	0.1634(1)	0.0139(2)
Sb8	4*c*	0.50	0.1894(1)	1/4	0.1611(1)	0.0108(2)

[a] U_{eq} is defined as one-third of the trace of the orthogonalized U_{ij} tensor.

formula of $Tb_2Ti_{10.4}Sb_{14.6}$. In the Yb compound, the *M*2 site contains 0.79 Ti and 0.21 Sb, corresponding to an overall formula of $Yb_2Ti_{10.6}Sb_{14.4}$.

Atomic positions were standardized with the program *STRUCTURE TIDY*.[8] Final values of the positional and displacement parameters are given in Table 2. Selected interatomic distances are listed in Table 3. Further data, in the form of crystallographic information files (CIFs), are available as Supporting Information or may be obtained from Fachinformationszentrum Karlsruhe, Abt. PROKA, 76344 Eggenstein-Leopoldshafen, Germany (No. CSD-419637 to 419639).

Electrical Resistivity. Block-shaped single crystals of $Sm_2Ti_{11}Sb_{14}$ and $Yb_2Ti_{10.6}Sb_{14.4}$ were selected for electrical resistivity measurements after their identities were confirmed by EDX analysis. Given the small dimensions of these crystals, only two-probe measurements were made on a Quantum Design Physical Property Measurement System (PPMS) equipped with an ac transport controller (Model 7100) from 2 to 300 K. The current was 100 μA and the frequency was 16 Hz. Measurements were performed twice to confirm reproducibility.

Results and Discussion

The structure of $RE_2Ti_{11-x}Sb_{14+x}$ (RE = Sm, Gd, Tb, Yb) is quite complex, exhibiting several types of disorder: (i) split Sb sites, (ii) partial occupancy of one of the Ti sites, and (iii) mixing of Ti and Sb atoms. For simplicity, we first examine the structure of $Sm_2Ti_{11}Sb_{14}$, which exhibits only the first two types of disorder. Figure 1 shows the three-dimensional framework assembled by linking Ti-centered polyhedra with Sb atoms at the vertices, yielding cavities that are filled with Sm atoms. Within the two sets of split, half-occupied Sb sites (Sb5/Sb6 and Sb7/Sb8), only one member of each set is portrayed. There are five distinct Ti sites, one (Ti3) centered within octahedra ($TiSb_6$, CN6) and four (Ti1, Ti2, Ti4, Ti5) within pentagonal bipyramids ($TiSb_7$, CN7). Chains are formed that extend along the *b* direction by sharing opposite faces of the titanium-centered

(8) Gelato, L. M.; Parthé, E. *J. Appl. Crystallogr.* **1987**, *20*, 139–143.

Table 3. Selected Interatomic Distances (Angstroms) in $RE_2Ti_{11-x}Sb_{14+x}$ (RE = Sm, Tb, Yb)[a]

	$Sm_2Ti_{11}Sb_{14}$	$Tb_2Ti_{10.41(1)}Sb_{14.59(1)}$	$Yb_2Ti_{10.58(1)}Sb_{14.42(1)}$
RE−Sb5/Sb6	3.076(2)/3.212(2)	3.055(5)/3.196(5)	3.088(3)/3.218(3)
RE−Sb8/Sb7	3.122(1)/3.510(1)	3.089(2)/3.495(2)	3.114(1)/3.551(1)
RE−Sb3 (×2)	3.1231(2)	3.1084(4)	3.1348(2)
RE−Sb1	3.1569(4)	3.1440(7)	3.1528(5)
RE−Sb4 (×2)	3.2228(3)	3.2121(6)	3.2303(4)
RE−Sb4 (×2)	3.2462(3)	3.2333(6)	3.2415(4)
Ti1−Sb2	2.7062(9)	2.699(2)	2.7213(10)
Ti1−Sb1	2.7324(8)	2.730(2)	2.7237(10)
Ti1−Sb4 (×2)	2.9395(8)	2.965(1)	2.9509(9)
Ti1−Sb7/Sb8 (×2)	2.9624(4)/3.0722(5)	2.955(1)/3.072(1)	2.9543(4)/3.0768(6)
Ti1−Sb3	3.0058(9)	3.011(2)	2.988(1)
*M*2−Sb2	2.7330(9)	2.788(2)	2.8350(8)
*M*2−Sb4 (×2)	2.8481(7)	2.858(1)	2.8573(7)
*M*2−Sb1	2.8776(9)	2.885(2)	2.8793(8)
*M*2−Sb3	2.9441(9)	2.914(2)	2.9157(9)
*M*2−Sb6/Sb5 (×2)	2.9665(7)/3.0611(8)	2.987(2)/3.054(2)	2.9972(9)/3.0599(10)
*M*3−Sb7/Sb8	2.735(1)/2.782(1)	2.738(3)/2.788(3)	2.734(1)/2.782(1)
*M*3−Sb6/Sb5	2.780(2)/2.880(2)	2.793(4)/2.898(4)	2.790(3)/2.892(2)
*M*3−Sb1	2.7884(6)	2.787(1)	2.7816(7)
*M*3−Sb2	2.8691(6)	2.878(1)	2.8846(8)
*M*3−Sb2	2.8761(6)	2.882(1)	2.8903(8)
*M*3-Sb3	2.9139(6)	2.914(1)	2.9049(8)
Ti4−Sb8/Sb7	2.708(2)/2.726(2)	2.719(3)/2.735(3)	2.716(2)/2.723(2)
Ti4−Sb3	2.7938(8)	2.781(2)	2.785(1)
Ti4−Sb5/Sb6	2.794(2)/3.061(2)	2.793(4)/3.065(4)	2.785(3)/3.058(2)
Ti4−Sb4 (×2)	2.8599(7)	2.857(1)	2.8568(9)
Ti4−Sb1 (×2)	3.0367(3)	3.0261(6)	3.0334(4)
Ti5−Sb7/Sb8	[2.300(2)]/2.720(2)	[2.302(4)]/2.741(3)	[2.296(2)]/2.765(2)
Ti5−Sb6/Sb5	[2.359(2)]/2.715(2)	[2.369(4)]/2.738(4)	[2.391(3)]/2.753(2)
Ti5−Sb2	2.790(2)	2.799(3)	2.832(2)
Ti5−Sb2 (×2)	3.0948(8)	3.093(1)	3.1008(8)
Ti5−Sb4 (×2)	3.150(2)	3.160(3)	3.110(2)
Ti1-*M*3 (× 2)	3.190(1)	3.176(2)	3.190(1)
*M*3−*M*3	2.774(1)	2.761(2)	2.786(1)
*M*3−*M*3	2.942(1)	2.943(2)	2.927(1)
Sb2−Sb2 (×2)	3.2803(3)	3.2740(6)	3.2903(4)
Sb4−Sb4	2.8572(4)	2.8492(9)	2.8494(5)
Sb4−Sb4	2.8592(4)	2.8544(9)	2.8641(5)
Sb5−Sb8	3.094(2)	3.040(4)	3.051(2)

[a] Sites *M*2 and *M*3 contain a mixture of titanium and antimony whose proportions depend on the *RE* member (Table 2). Split sites Sb5/Sb6 and Sb7/Sb8 are each half-occupied.

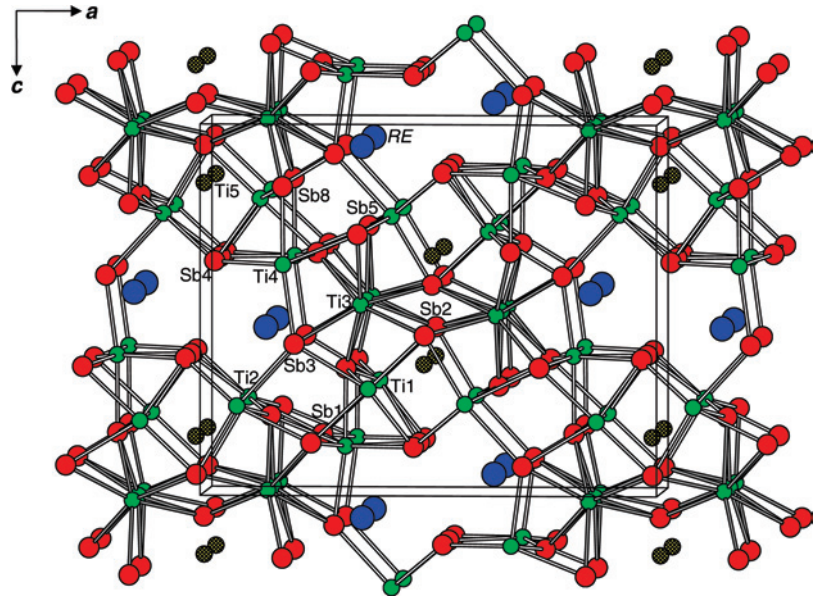

Figure 1. Structure of $RE_2Ti_{11-x}Sb_{14+x}$ (RE = Sm, Tb, Yb) viewed down the *b* direction, emphasizing the Ti−Sb framework. The large blue circles are *RE* atoms, the small green circles are titanium atoms, and the medium red circles are antimony atoms. In the split sites Sb5/Sb6 and Sb7/Sb8, only one member of each set is shown.

octahedra or by sharing equatorial vertices of the titanium-centered pentagonal bipyramids (Figure 2). The source of the disorder becomes apparent upon inspection of the chains containing the Ti5 sites, which are only half-occupied. In

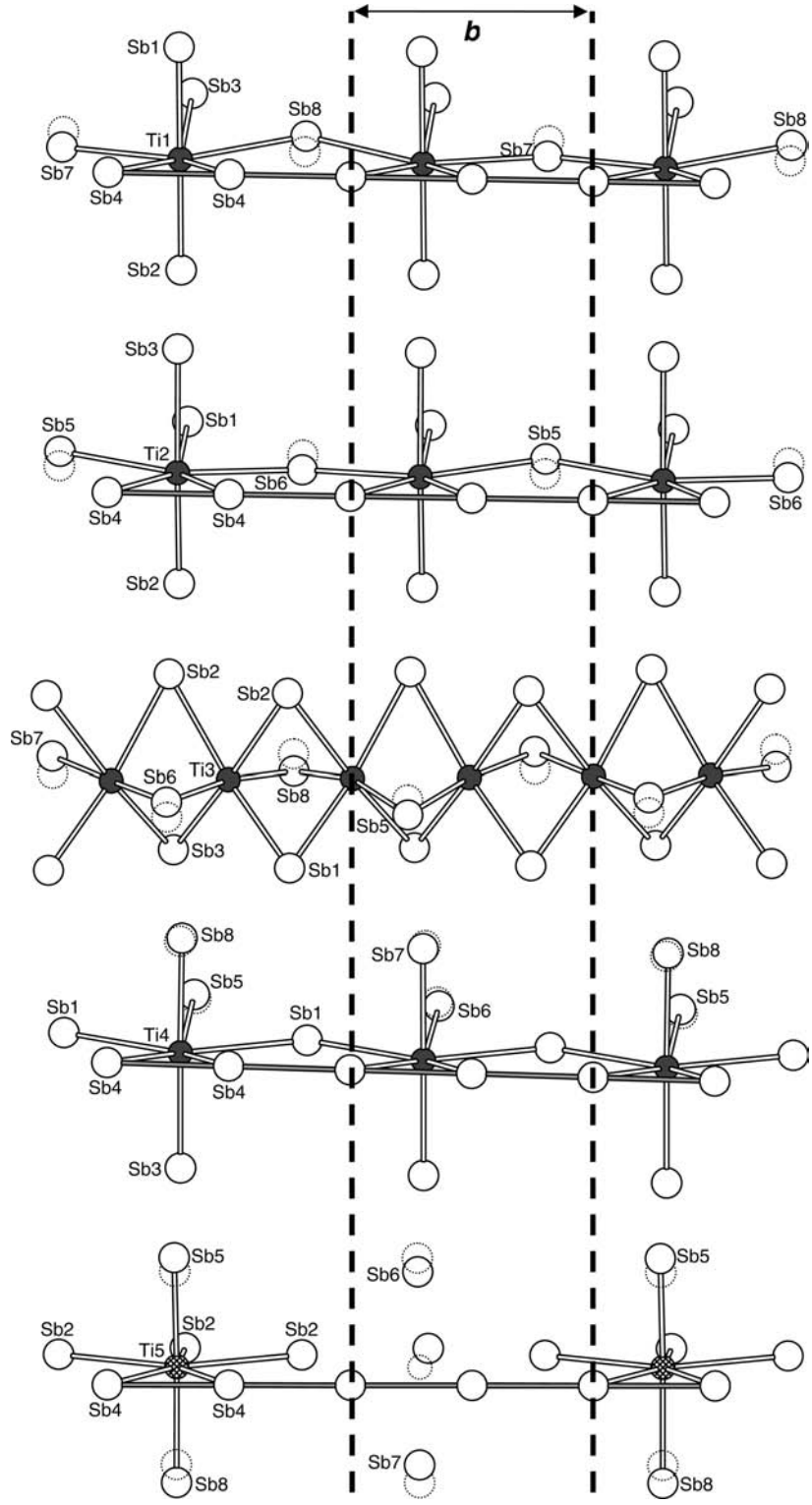

Figure 2. Chains of Ti-centered pentagonal bipyramids or octahedra extending down the *b* direction, with possible local orderings of the split Sb sites (Sb5/Sb6 and Sb7/Sb8) and half-occupied Ti5 site.

the other chains, the distances from the titanium centers to the antimony sites (including the half-occupied ones) are 2.7−3.0 Å, in good agreement with the sum of the Pauling radii (2.715 Å)[9] and with similar distances in $La_2Ti_7Sb_{12}$ (2.7373(4)−2.8785(6) Å).[6] In contrast, the half-occupancy of the Ti5 site arises because of the need to maintain reasonable Ti5−Sb distances: if Ti5 is occupied, the axial sites occupied must be Sb5 and Sb8 (2.715(2)−2.720(2) Å) but not Sb6 and Sb7 (2.300(2)−2.359(2) Å); if Ti5 is vacant, the axial sites can relax to Sb6 and Sb7. In principle, long-range ordering of the Ti5 atoms could develop within this chain, corresponding to a superstructure along *b*, but different

(9) Pauling, L. *The Nature of the Chemical Bond*, 3rd ed.; Cornell University Press: Ithaca, NY, 1960.

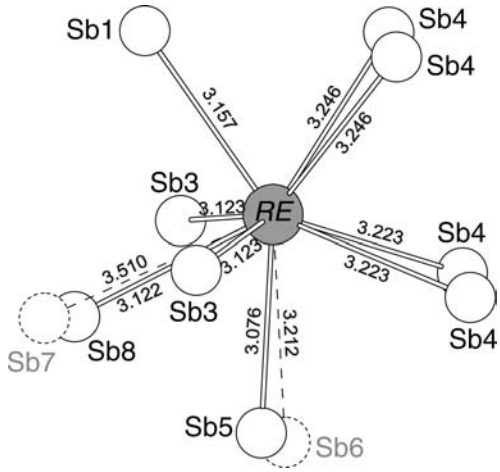

Figure 3. Monocapped square antiprismatic coordination around *RE* atom in $RE_2Ti_{11-x}Sb_{14+x}$ (*RE* = Sm, Tb, Yb). Distances shown (in Å) are for $Sm_2Ti_{11}Sb_{14}$.

chains need not be in registry, leading to the observed average disordered structure. Associated with this disorder is the coordination environment around the samarium atom (Figure 3). The geometry is nine-coordinate, in the form of a monocapped square antiprism (the squares being Sb4−Sb4−Sb4−Sb4 and Sb3−Sb1−Sb3−Sb5/Sb6, and the cap being Sb8/Sb7). The Sm−Sb5 and Sm−Sb8 distances are the shortest (3.076(2) and 3.122(1) Å, respectively) within the polyhedron, at the lower limit of reasonable Sm−Sb contacts (cf. 3.13(2)−3.48(2) Å in $SmSb_2$ and 3.14 Å in SmSb).[10,11] Occupation of the alternate antimony sites allows a more reasonable Sm−Sb6 distance to be recovered (3.212(2) Å) but considerably lengthens the Sm−Sb7 distance (3.510(1) Å). The occurrence of split antimony sites may thus be attributed to a structural compromise to balance the competing needs to achieve reasonable Ti5−Sb and Sm−Sb contacts.

The separation between titanium sites corresponds to approximately half of the *b* parameter in the face-sharing octahedral chains or exactly the *b* parameter in the vertex-sharing pentagonal bipyramidal chains (Figure 2). The Ti3−Ti3 distances (2.774(1)−2.942(1) Å) within the face-sharing octahedral chains are similar to those found in related structure of $Ti_{11-x}Sb_{8-y}$ (2.707(4)−2.890(4) Å) where metal−metal bonding interactions have been confirmed to be present.[12] Common to all the vertex-sharing pentagonal bipyramidal chains, the Sb4 atoms form a linear skewer with 2.8572(4)−2.8592(4) Å distances also suggestive of Sb−Sb bonding.

The full 3D structure is densely packed and may be built up from alternately stacking two types of slabs along the *c* direction (Figure 4). At $z = 0$ and $^1/_2$, the slabs consist of double chains of face-sharing Ti3-centered octahedra and of *RE*-centered polyhedra. At $z = {}^1/_4$ and $^3/_4$, the slabs consist of double chains of Ti1- and Ti2-centered pentagonal pyramids. Within this arrangement of densely packed polyhedra, the remaining voids are then either fully occupied by Ti4 atoms or half-occupied by Ti5 atoms.

The clear demarcation of $RE_2Ti_{11-x}Sb_{14+x}$ (*RE* = Sm, Gd, Tb, Yb) from $RE_2Ti_7Sb_{12}$ (*RE* = La, Ce, Pr, Nd) suggests that there are critical limits on the size of the *RE* atom. In both cases, the *RE* atoms are surrounded by antimony atoms in nine-coordinate geometry, but the *RE*−Sb distances decrease significantly from $RE_2Ti_7Sb_{12}$ (e.g., 3.205(1)−3.471(1)

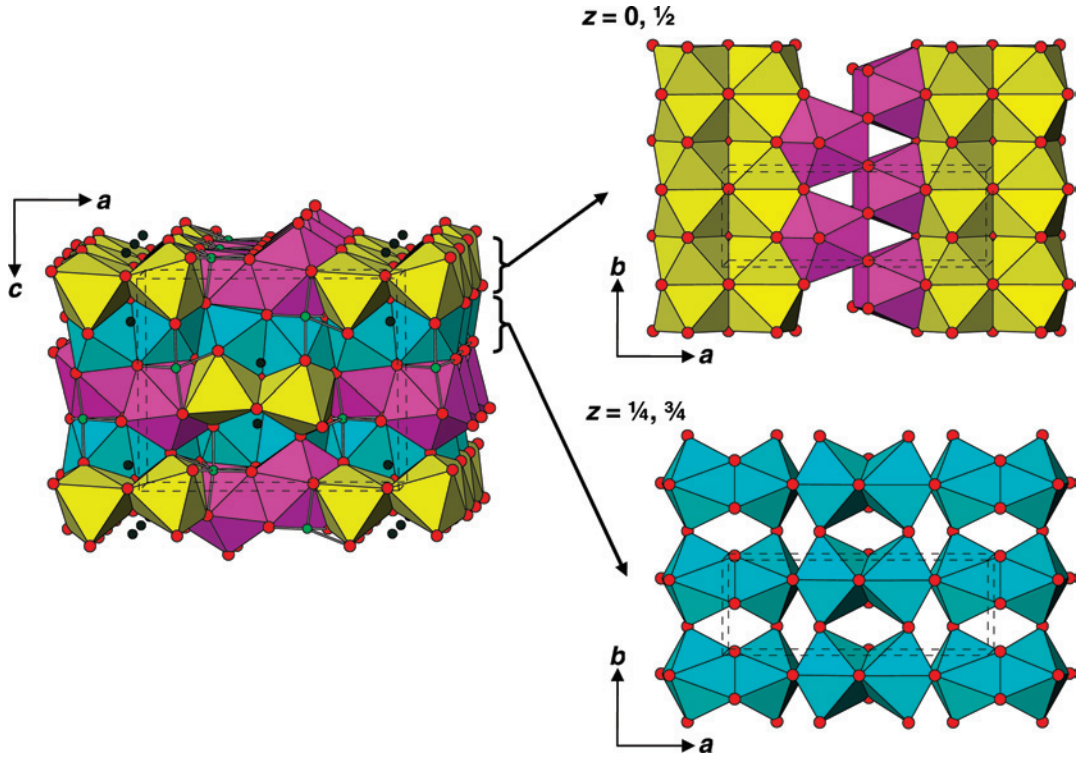

Figure 4. Structure of $RE_2Ti_{11-x}Sb_{14+x}$ (*RE* = Sm, Tb, Yb) in terms of 2D slabs alternately stacked along the *c* direction consisting of (i) Ti3-centered octahedra (yellow) and *RE*-centered monocapped square antiprisms (magenta) (at $z = 0, {}^1/_2$) or (ii) Ti1- and Ti2-centered pentagonal bipyramids (cyan) (at $z = {}^1/_4, {}^3/_4$). Remaining voids are filled by Ti4 and Ti5 atoms.

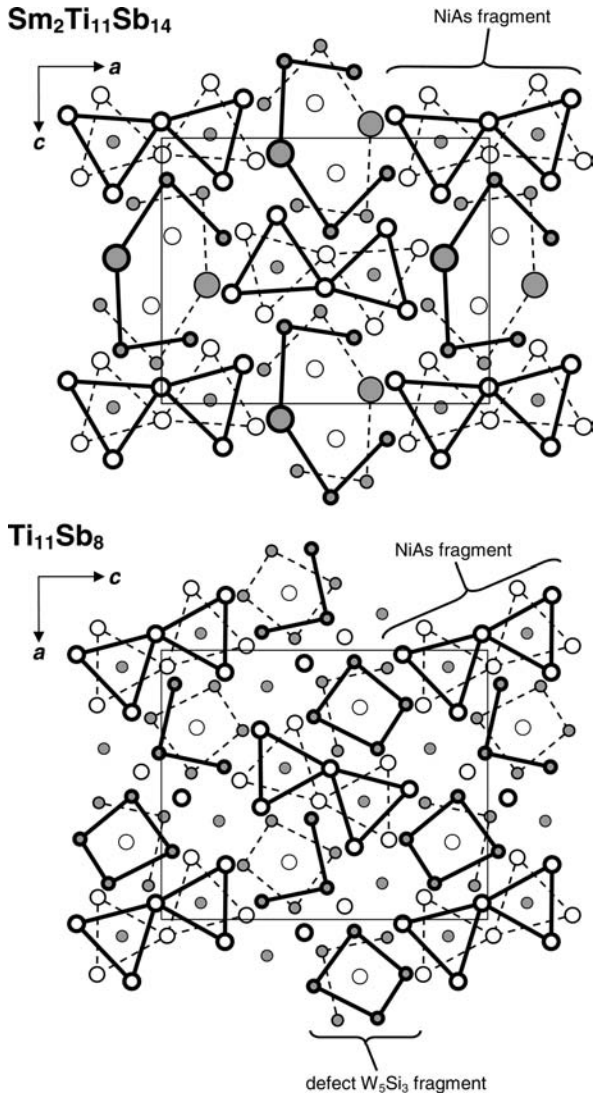

Figure 5. Comparison of the structures of $Sm_2Ti_{11}Sb_{14}$ and $Ti_{11}Sb_8$, in terms of nets at $y = {}^1/_4$ (thick lines) or $y = {}^3/_4$ (thin lines), with titanium and antimony atoms at $y = \sim 0$ and $\sim {}^1/_2$. The large shaded circles are samarium atoms, the small shaded circles are titanium atoms, and the medium open circles are antimony atoms.

Å in $La_2Ti_7Sb_{12}$)[6] to $RE_2Ti_{11-x}Sb_{14+x}$ (e.g., 3.088(3)−3.2415(4) Å in $Sm_2Ti_{11}Sb_{14}$), a manifestation of the lanthanide contraction. Substitution of samarium with later rare-earth metals induces an additional disorder involving mixing of titanium and antimony atoms, giving the formulas $Tb_2Ti_{10.4}Sb_{14.6}$ and $Yb_2Ti_{10.6}Sb_{14.4}$. The substitution of such seemingly chemically disparate elements for each other may seem surprising, even though titanium and antimony are not too dissimilar in size (with metallic radii R_1 of 1.324 and 1.391 Å, respectively).[9] However, this type of disorder is now emerging to be a recurring feature of several transition-metal antimonides such as $Ti_{11-x}Sb_{8-y}$,[12] $Hf_6Ni_{1-x}Sb_{2+x}$,[13] $Zr_5M_{1-x}Sb_{2+x}$ (M = Fe, Co, Ni),[14] and $Hf_{10}M_xSb_{6-x}$ (M = V−Cu),[15] and points to the importance of size effects in controlling the stability of these structures. In $Tb_2Ti_{10.4}Sb_{14.6}$, 15% of the atoms in the Ti3 site are replaced by slightly larger antimony atoms, which could be interpreted as a counteracting response against an overall contraction of the structure. In $Yb_2Ti_{10.6}Sb_{14.4}$, 21% of the atoms in a different site, Ti2, are

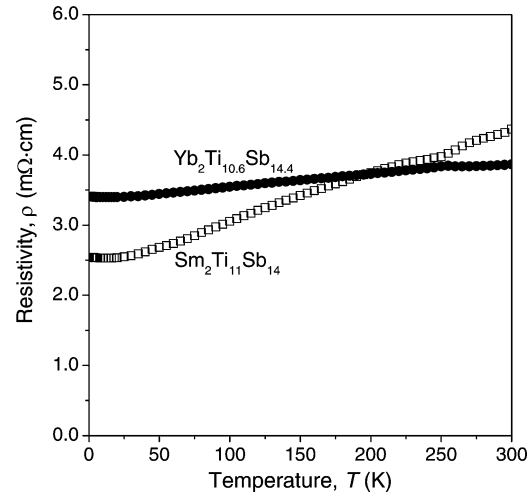

Figure 6. Electrical resistivity of single crystals of $Sm_2Ti_{11}Sb_{14}$ and $Yb_2Ti_{10.6}Sb_{14.4}$.

replaced by antimony atoms, and interestingly, the cell parameters and bond distances have now increased (relative to $Tb_2Ti_{10.4}Sb_{14.6}$). The interruption of the $RE_2Ti_{11-x}Sb_{14+x}$ series after RE = Tb and its resumption at RE = Yb argues strongly for the presence of divalent ytterbium, in contrast to trivalent RE for the other members, to offset the structural contraction. (The trend in size can be inferred from the Shannon−Prewitt (ionic) radii for RE^{3+} (CN9), which decrease from 1.36 to 1.30 Å for La^{3+} to Nd^{3+}, 1.27 to 1.24 Å for Sm^{3+} to Tb^{3+}, and then to 1.18 Å for Yb^{3+}.[16] The radius for Yb^{2+} (only specified up to CN8) is 1.28 Å.) The $RE_2Ti_{11-x}Sb_{14+x}$ structure thus appears to be stable only within a rather limited range of permitted RE sizes. It remains unclear why the site preference for the antimony admixture differs in the terbium versus ytterbium members; indeed both sites might be simultaneously susceptible to this mixing, giving rise to a limited range of solid solubility. Because the original syntheses were performed with a deficiency of titanium and antimony relative to the final refined compositions, and the weight loss from antimony volatilization that occurs during arc-melting is variable (typically ranging from ~3 to ~8 wt %), the final composition that is attained may well differ depending on the synthetic conditions. If the Ti2 and Ti3 sites are assumed to be the only ones that can accommodate mixing with antimony atoms, to a maximum of 50%, then the limits of solid solubility in $RE_2Ti_{11-x}Sb_{14+x}$ can be estimated to lie within the range $0 < x < 3$.

Although the structure of $RE_2Ti_{11-x}Sb_{14+x}$ is unique, parts of it are modestly related to other structures, such as $Ti_{11}Sb_8$ (Figure 5).[12] The double chains of face-sharing titanium-centered octahedra extending along the b direction are a familiar motif, forming a fragment of the NiAs-type structure. In $Ti_{11}Sb_8$, these NiAs-type fragments are intergrown with defect W_5Si_3-type fragments in which one of the corners is missing from each of the antimony-centered square antiprisms, $SbTi_7\square_1$, which share opposite square faces within chains extending along the b direction as well. In $Sm_2Ti_{11}Sb_{14}$, these defect W_5Si_3-type fragments have become fused and one of the corners is replaced by Sm, $Sb_2Ti_4Sm_1\square_1$. Although this comparison should not be taken too far, it is

useful in highlighting the development along the *b* direction of linear skewers of titanium or antimony atoms, which center these polyhedra, in both structures. By extension, many of the conclusions derived from band structure calculations on $Ti_{11}Sb_8$ would also apply to $Sm_2Ti_{11}Sb_{14}$. The titanium and antimony skewers are in close registry with each other, with homoatomic contacts of ~2.8 Å. These distances correspond to strong and nearly optimized Ti−Ti bonding but are misleadingly short to imply classical 2c−2e$^-$ Sb−Sb bonding. Rather, the short Sb−Sb distances are imposed by matrix effects defined by the rest of the structure and correspond more closely to delocalized hypervalent 2c−1e$^-$ bonds.

Resistivity measurements on $Sm_2Ti_{11}Sb_{14}$and $Yb_2Ti_{10.6}Sb_{14}$ reveal typical metallic behavior (Figure 6), with only a very weak dependence on temperature characteristic of disordered materials. In $Sm_2Ti_{11}Sb_{14}$, the resistivity ratio is already quite low ($\rho_{300}/\rho_2 = 1.7$), whereas in $Yb_2Ti_{10.6}Sb_{14.4}$, the resistivity is nearly temperature-independent ($\rho_{300}/\rho_2 = 1.1$), consistent with significant scattering of conduction electrons by defects.

$RE_2Ti_{11-x}Sb_{14+x}$ (*RE* = Sm, Gd, Tb, Yb) extends the body of known ternary phases in the *RE*−Ti−Sb systems, which was previously restricted to RE_3TiSb_5 (La−Nd, Sm) and $RE_2Ti_7Sb_{12}$ (La−Nd). Homoatomic Ti−Ti and Sb−Sb bonding interactions are an important component in the structures of all these phases, but disorder between titanium and antimony atoms can ensue in response to size demands of the *RE* component. Further work is in progress to examine the remaining ternary systems containing the late *RE* metals.

Acknowledgment. The Natural Sciences and Engineering Research Council of Canada and the University of Alberta supported this work. We thank Dr. Robert McDonald and Dr. Michael J. Ferguson (X-ray Crystallography Laboratory) for the X-ray data collection and Ms. Christina Barker (Department of Chemical and Materials Engineering) for assistance with the EDX analysis.

Supporting Information Available: X-ray crystallographic files in CIF format. This material is available free of charge via the Internet at http://pubs.acs.org.

IC800317C

(10) Wang, R.; Steinfink, H. *Inorg. Chem.* **1967**, *6*, 1685–1692.
(11) Iandelli, A. *Z. Anorg. Allg. Chem.* **1956**, *288*, 81–86.
(12) Bobev, S.; Kleinke, H. *Chem. Mater.* **2003**, *15*, 3523–3529.
(13) Kleinke, H. *J. Alloys Compd.* **1998**, *270*, 136–141.
(14) Kwon, Y.-U.; Sevov, S. C.; Corbett, J. D. *Chem. Mater.* **1990**, *2*, 550–556.
(15) Kleinke, H.; Ruckert, C.; Felser, C. *Eur. J. Inorg. Chem.* **2000**, 315–322.
(16) Shannon, R. D. *Acta Crystallogr., Sect. A* **1976**, *32*, 751–767.